Open access • Journal Article • DOI:10.1007/S10652-015-9432-1

Resistance and reconfiguration of natural flexible submerged vegetation in hydrodynamic river modelling — Source link

Veerle Verschoren, Dieter Meire, Jonas Schoelynck, Kerst Buis ...+5 more authors

Institutions: University of Antwerp, Ghent University, University of Limpopo

Published on: 01 Feb 2016 - Environmental Fluid Mechanics (Springer Netherlands)

Topics: Hydraulic roughness and Flume

Environ Fluid Mech
DOI 10.1007/s10652-015-9432-1

ORIGINAL ARTICLE

Resistance and reconfiguration of natural flexible submerged vegetation in hydrodynamic river modelling

Veerle Verschoren[1] · Dieter Meire[2,3] · Jonas Schoelynck[1] · Kerst Buis[1] · Kris D Bal[1,4] · Peter Troch[2] · Patrick Meire[1] · Stijn Temmerman[1]

Received: 3 December 2014 / Accepted: 19 October 2015

Abstract In-stream submerged macrophytes have a complex morphology and several species are not rigid, but are flexible and reconfigure along with the major flow direction to avoid potential damage at high stream velocities. However, in numerical hydrodynamic models, they are often simplified to rigid sticks. In this study hydraulic resistance of vegetation is represented by an adapted bottom friction coefficient and is calculated using an existing two layer formulation for which the input parameters were adjusted to account for (i) the temporary reconfiguration based on an empirical relationship between deflected vegetation height and upstream depth-averaged velocity, and (ii) the complex morphology of natural, flexible, submerged macrophytes. The main advantage of this approach is that it removes the need for calibration of the vegetation resistance coefficient. The calculated hydraulic roughness is an input of the hydrodynamic model Telemac 2D, this model simulates depth-averaged stream velocities in and around individual vegetation patches. Firstly, the model was successfully validated against observed data of a laboratory flume experiment with three macrophyte species at three discharges. Secondly, the effect of reconfiguration was tested by modelling an in situ field flume experiment with, and without, the inclusion of macrophyte reconfiguration. The inclusion of reconfiguration decreased the calculated hydraulic roughness which resulted in smaller spatial variations of simulated stream velocities, as compared to the model scenario without macrophyte reconfiguration. We discuss that including macrophyte reconfiguration in numerical models input, can have significant and extensive effects on the model results of hydrodynamic variables and associated ecological and geomorphological parameters.

✉ Veerle Verschoren
veerle.verschoren@uantwerpen.be

[1] Department of Biology, Ecosystem Management Research Group, University of Antwerp, Wilrijk, Belgium

[2] Hydraulics Laboratory, Department of Civil Engineering, Ghent University, Ghent, Belgium

[3] Flanders Hydraulics Research, Antwerp, Belgium

[4] Department of Biodiversity, University of Limpopo, Sovenga, South Africa

Published online: 27 October 2015

Keywords Open-channel flow · Roughness · Macrophytes · 2D modelling · Stream ecosystem

Abbreviations

A_C	Characteristic area of the plant (m^2)
A_w	Total wetted plant surface (m^2 m^{-2})
b	Vogel exponent (–)
C_b	Chézy coefficient of the bed ($m^{1/2}$ s^{-1})
C_D	Drag coefficient (–)
C_D'	Modified drag coefficient to account for flexible vegetation (–)
$C_{D,exp}$	Experimental drag coefficient (–)
C_r	Representative Chézy value for vegetation ($m^{1/2}$ s^{-1})
D	Cylinder diameter (m)
F_D	Drag force of the vegetation (N)
g	Gravitational acceleration (m s^{-2})
h	Water depth (m)
k	Vegetation height (m)
k_u	Variable vegetation height in function of stream velocity (m)
L_{cp}	Shoot height of *Callitriche platycarpa* (m)
L_{pp}	Shoot height of *Potamogeton pectinatus* (m)
L_{pn}	Shoot height of *Potamogeton natans* (m)
m	Number of cylinders per m^2 horizontal area (m^{-2})
n	Manning coefficient (s $m^{-1/3}$)
NS	Nash-Sutcliffe coefficient (–)
Q	Discharge (m^3 s^{-1})
R	Hydraulic radius (m)
S	Water level slope (–)
U	Flow velocity (m s^{-1})
α	Angle with horizontal bed and shoot (°)
ρ	Density of water (kg m^{-3})
κ	Von Kármán constant (–)

1 Introduction

In-stream macrophytes (aquatic vegetation) increase the resistance encountered by river flow [1]. Concomitantly, it has been shown that configurations of macrophyte patches and non-vegetated zones cause local decreased flow velocity within vegetation patches and local increased flow velocity right next to the vegetation patches [2, 3]; as well as overall increased water levels, compared to vegetation free parts of the river [4]. The water flow, in turn, creates drag force on the vegetation [5, 6]. These mutual plant-flow interactions have important effects on the hydraulic, ecological and geomorphic functioning of lowland rivers [7–9] and it is therefore crucial to implement plant-flow interactions in hydrodynamic models.

Plant-flow interactions have been relatively well studied in recent years through numerical modelling [10, 11], laboratory experiments [12–15] and field measurements [8, 16]. Vegetation resistance can be quantified via empirical relationships or with

hydrodynamic models. In the empirical approach, the overall resistance in a vegetated reach is determined via the relationship between biomass and resistance, [17, 18] or between blockage factors and resistance [19]. However, it has been demonstrated that hydraulic resistance is also influenced by discharge; and several authors have investigated n-UR relationships [20–23]. The Manning coefficient, n (m $s^{-1/3}$), quantifies the overall hydraulic resistance in a river reach and depends on flow velocity, U (m s^{-1}), and hydraulic radius, R (m), with the latter being the ratio of the cross-sectional area to the wetted perimeter. Several approaches, based on this Manning equation, are derived to estimate the hydraulic resistance caused by submerged vegetation and have been implemented into hydrodynamic models [e.g. 1, 10, 11, 24, 25], see for Vargas-Luna et al. [26] a comparative analysis. These equations divide the vertical velocity profile into two layers: one layer within the vegetation canopy and one layer above the vegetation canopy. The relative contribution of both layers depends on the vegetation height. Therefore, in this study the reconfiguration is described by the temporary bending of the vegetation, which results in varying vegetation height in function of stream velocity. Previous studies described the reconfiguration of vegetation by the reduction in frontal area (A) and streamlining (C_D, drag coefficient) [27].

Nevertheless, there is a gap between the theoretical understanding and description of hydraulic resistance, caused by vegetation and common botanical measurements, used in practice [28]. The vegetation is often represented by simple, rigid sticks in experiments [29–31] and modeled as such [11, 32]. Yet, we identify two main difficulties when dealing with natural, flexible macrophytes: (i) including the flexible structure, and (ii) quantifying the species' complex morphology. Firstly, in attempts to better mimic the flexibility of plants in a natural situation, researchers have used rice shoots [33] or alfalfa seedlings [34], instead of artificial, rigid plant structures. Yet these are still emergent objects, while many of the in-stream macrophytes grow typically submerged and interact with the flow to a great extent [35]. Submerged macrophytes have their entire canopy in the water column and experience a drag force, which consists of form drag and friction drag [28]. Due to the buoyancy and the stiffness of the macrophytes, the canopy stays in an upright position [36]. At higher stream velocities, the flow-induced drag force pushes the macrophytes in a more downward position [37]. Their morphology is therefore often flexible and streamlined to enable temporary reconfiguration of the canopy and to avoid potential damage at high stream velocities [38]. Models for submersed, flexible vegetation, for which the whole bed is homogeneously covered with vegetation exist [39, 40]. Dijkstra [39] modeled the bending of flexible seagrass and flexible plastic strips based on biophysical processes, including vegetation position and buoyancy. Luhar, Nepf [41] calculated the plant posture of flexible seagrass using the force balance between posture-dependent drag and restoring forces, due to vegetation stiffness and buoyancy. However, in rivers and streams a patchy vegetation pattern is often observed, where zones with vegetation alternates with bare sediment, or with vegetated zones of a different species [38]. Experiments with flexible vegetation patches have been executed by e.g. [12, 42–44]. Secondly, the morphology of the vegetation is traditionally represented by the stem diameter and number of stems per unit horizontal area. These parameters can be measured relatively easily for single branched species; but for broadly branched species with many leaves it is difficult to quantify these parameters. We lump therefore, in this paper, these parameters into the plant surface area; this approach is similar to the method suggested by Aberle, Jarvela [45] where the leaf area index is used.

The aim of this study is to derive a practical approach to quantify vegetation resistance which can be applied in 2D depth-averaged models on reach scale. By using a 2D model

we are able to investigate spatial heterogeneous vegetation patterns on reach scale. Future applications can include the effect of different spatial vegetation patterns on the overall hydraulic resistance, the impact of spatio-temporal vegetation dynamics on the flow field, habitat suitability for macro-invertebrates, optimisation of flood management, etc.

Quantification of the hydraulic resistance created by the vegetation needs to account for the ability of flexible macrophytes to temporary reconfigure their canopy with the flow and the complex morphology of natural plants. The calculated hydraulic resistance induced by flexible macrophytes will depend on whether or not the model accounts for temporary reconfiguration. Consequently, this gives rise to differences in depth-averaged velocity distribution; hence affecting results on associated hydraulic, ecological and geomorphological processes. The lack of correct implementation of vegetation resistance, based on common botanical parameters and a variable vegetation height, is a structural shortcoming in contemporary hydrodynamic models, when dealing with natural in-stream macrophytes. Two research questions are addressed in this study;

(i) How to estimate the hydraulic resistance of in-stream macrophyte patches including temporary reconfiguration and based on measurable plant parameters? And is the resulting simulated flow field in agreement with the observed flow field?
(ii) What is the effect of inclusion or exclusion of macrophyte reconfiguration on the modeled flow field?

We demonstrate that if reconfiguration is not included, the hydraulic resistance can be overestimated, often resulting in incorrect flow velocities. These research questions are addressed with the 2D hydrodynamic model Telemac 2D [46]. The modelling of a laboratory flume experiment performed by Bal et al. [4] is used to address the first research question. The second research question is answered by modelling an in situ field flume experiment executed by Schoelynck et al. [38]. Both experiments are selected because natural, flexible, aquatic vegetation is used and stream velocities in and around the vegetation patch are recorded in detail.

2 Materials and methods

In this study we extend a resistance estimation method for vegetation to calculate the representative Chézy value of in-stream macrophytes. We formulate appropriate plant parameters to account for the flexible and complex structure of the vegetation. These parameters are quantified for three target species. The hydrodynamic model and calculation scheme is described. Finally, the experimental setup of the two case studies is summarised.

2.1 Parameter formulation

Vargas-Luna et al. [26] performed a comparative analysis and validation of fourteen models which describe the resistance effect caused by aquatic vegetation. Here we built further upon the approach proposed by Baptist et al. [1] (Eq. 1), which was identified by Vargas-Luna et al. [26] as one of the model approaches that performs best to simulate both submerged and emerged vegetation, real and artificial vegetation, and rigid and flexible vegetation. It is important that the vegetation height in the formula corresponds to the deflected vegetation height in the field [47]; therefore in this study we consider reconfiguration as a varying deflected vegetation height in function of stream velocity.

Furthermore, (Eq. 1) is successfully used in other studies with real vegetation: such as the simulation of the flow field over a river floodplain with grass, reed and softwood [48, 49], and marsh vegetation [50]. Following the approach of Baptist et al. [1], the representative Chézy value at every location with vegetation is described by (Eq. 1):

$$C_r = \sqrt{\frac{1}{1/C_b^2 + (kmDC_D)/(2g)}} + \frac{\sqrt{g}}{\kappa} \ln\left(\frac{h}{k}\right) \tag{1}$$

Equation 1 assumes a uniform flow velocity through the fully submerged vegetation and a logarithmic profile above the vegetation [1]. The first term in (Eq. 1) represents the resistance created by the river bed and within the vegetation canopy. The second term accounts for the vegetation-free flowing zone above the canopy. The resistance created by the vegetation depends on the following plant parameters: canopy height, k (m), number of stems per unit horizontal area, m (m^{-2}), diameter of the stems, D (m) and drag coefficient, C_D (–). The Chézy coefficient for the bed roughness (C_b) is obtained from standardised tables [51]; the Manning value found in these tables is converted into a Chézy coefficient by using the mean water depth of the domain. The gravitational acceleration (g) is 9.81 m s^{-2}, the Von Kármán constant (κ) is 0.4 and the water depth (h) is calculated in every grid cell. The representative Chézy value is used as an adapted bottom friction coefficient in the hydrodynamic model Telemac 2D.

In this research we study macrophyte patches that are flexible and consist of multiple individual shoots, which are woven into one another and can therefore not be identified individually. Hence, two adjustments on the input parameters are needed: (i) to account for the flexibility of the vegetation, the vegetation canopy height is varied as a function of the upstream depth-averaged velocity; and (ii) the complex morphology is represented by the total wetted surface area, A_w (m^2), of the plants. Firstly, in order to simulate the variation in vegetation canopy height, as a function of upstream depth-averaged velocity, a relationship between the bending angle and upstream depth-averaged velocity is used. The bending angle is defined as the angle between the horizontal bed and the shoot [13] (Fig. 1). The deflected vegetation height, k_u, which is the vegetation height after bending, is calculated as the product of the shoot height, L (m) and the sine of the bending angle (Table 1). The deflected shoot length is the product of the shoot height and the cosine of the bending angle. At lower velocities the deflected patch length is less reduced than the deflected shoot length, because the deflected patch length is impacted only by the shoots at the trailing end (Fig. 1).

Secondly, the complex morphology of stems and leaves is represented by replacing the product of the individual plant parameters, vegetation height, k (m), number of stems, m (m^{-2}), and stem diameter, D (m)—in (Eq. 1)—by the characteristic surface area, A_W (m^2 m^{-2}), of all plant structures (stems, leaves, etc.):

$$C_r = \sqrt{\frac{1}{1/C_b^2 + \left(A_W C_{D,\mathrm{exp}}\right)/(2g)}} + \frac{\sqrt{g}}{\kappa} \ln\left(\frac{h}{k_u}\right) \tag{2}$$

We do this because—as input for the model—it is not feasible to measure the individual plant parameters k, m and D on plant species with a complex morphology, while the characteristic area can be quantified as follows. For example, the leaf area index can be used, which is defined as the one-sided leaf area per horizontal area [45, 52, 53]. Another approach is the product of plant frontal area per canopy volume and vegetation height to

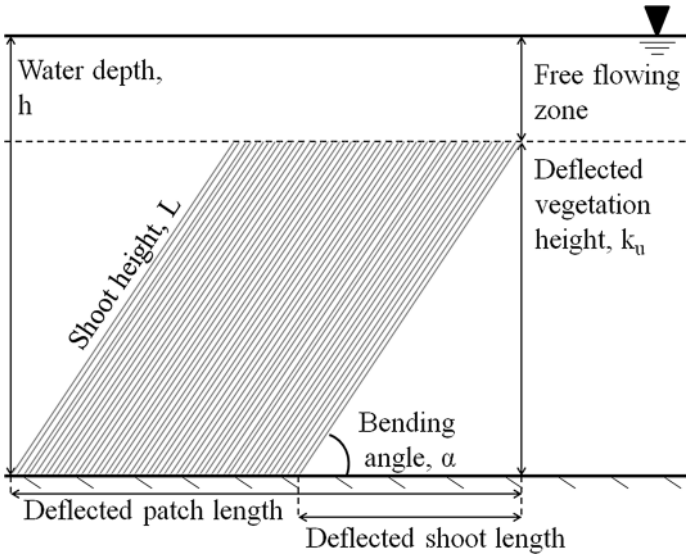

Fig. 1 Sketch showing a side-view of a flexible vegetation patch which consists of multiple shoots (*grey lines*). The deflected vegetation height depends on the upstream depth-averaged velocity, because the flow-induced drag force pushes the macrophyte in a downward position

Table 1 Plant parameters of the vegetation module, deflected vegetation height, bending angle (values from [13]), total wetted plant surface area per unit horizontal bed (field measurements of 2008 and 2013), bulk drag coefficient (values derived from [13])

Species	Deflected vegetation height k_u (m)	Bending angle α (°)	Wetted plant surface area A_W (m^2 m^{-2})	Experimental drag coefficient $C_{D,exp}$ (–)	Vogel exponent b (–)
C. platycarpa	L_{Cp} * sin (α)	$5.6*U^{-0.53}$	43.9 ± 20.4	0.034 ± 0.003	−1.09
P. pectinatus	L_{Pp} * sin (α)	$5.5*U^{-0.55}$	13.7 ± 0.8	0.054 ± 0.004	−0.78
P. natans	L_{Pn} * sin (α)	$8.7*U^{-0.60}$	8.5 ± 3.5	0.049 ± 0.004	−0.76

describe the characteristic area, A, in (Eq. 2) [54]. For flexible vegetation it is difficult to quantify the frontal area. Sand-Jensen [55] and Bal et al. [13] suggest to use the total wetted plant surface area. The wetted plant surface area of the vegetation is the total surface area of the vegetation canopy, which is in contact with the water, quantified per unit surface area of the river bed and is used in this study. It depends on the species and biomass but is independent of stream velocity and reconfiguration of the vegetation [55]. Therefore, this parameter can be quantified accurately and it accounts for the friction created by all plant structures including the stems and the leaves, which is important since leaves can account for 60 % of the total drag generated by macrophytes [13]. However, it should be noticed that the wetted plant surface area does not take into account the plant morphology itself.

2.2 Parameter estimation

Three submerged macrophyte species are used in this study: *Callitriche platycarpa,* Kütz (various-leaved water-starwort) is widely branched; *Potamogeton pectinatus,* L., also known as *Stuckenia pectinata* (sago pondweed) is ramified, but more streamlined than the former; and *Potamogeton natans*, L. (floating pondweed) is a single branched macrophyte with one leaf at the end of each shoot. *P. pectinatus* and *P. natans* have a similar stiffness and are less flexible than *C. platycarpa* [13].

An empirical relationship is used between the bending angle (α) and the upstream depth-averaged velocity based on published flume experiments of single shoots of the target species [13] (Table 1). In this published study, the bending angle was measured between the horizontal bed and the lowest 0.05 m of the shoot [13]. From the pictures that the authors took we can see that the bending angle along the whole length of the shoot is approximately constant. In our study, vegetation patches consisting of multiple shoots are modelled, therefore the bending angle of a single shoot is used as a proxy of the bending angle of all shoots in a whole patch (Fig. 1). We checked the reliability of this assumption by comparing the observed bending angle of *C. platycarpa* shoots [13] and patches [38] at three different velocities in published flume studies. The observed bending angles of shoots and patches were, respectively, 19° and 19°, 13° and 13°, 11° and 9° decimal degrees at stream velocities of 0.1, 0.2 and 0.3 m s^{-1}. The similarity can be explained by the mechanism that the leading edge of the patch pushes the whole canopy downwards under the same angle.

The wetted plant surface area is measured for the three target species. In total, nine vegetation samples of both *C. platycarpa* and *P. natans* were taken at peak biomass (June, July and August 2013) in two lowland rivers in north east Belgium. Biomass was sampled in plots of 0.25 m^2 with only the presence of the target species. Two samples of *P. pectinatus* were taken in the same rivers in 2008. The leaves and stems subsamples of each species were spread on a white background and photographed. Using ArcGIS 10.1 the surface area was determined. The wetted plant surface area was calculated using the dry weight of the subsample and the whole sample (Table 1).

Finally, the drag coefficient is quantified based on drag force measurements. In the first step, the drag coefficient is calculated with the generally accepted drag force equation (Eq. 3) [56]:

$$F_D = \frac{1}{2}\rho C_D A_C U^2 \tag{3}$$

with drag force, F_D (N), drag coefficient, C_D (−), density of water, ρ (kg m^{-3}), characteristic area of the object, A_c (m^2) and the stream velocity, U (m s^{-1}). Usually the characteristic area is defined as the projected area exposed to the flow [56], whereas in this study the wetted area is used for the same reasons as mentioned in paragraph (2.1). The flexible behaviour of vegetation in hydrodynamics can be accounted for by replacing C_D to C_D' in (Eq. 3) [57]. The modified drag coefficient, C_D', is calculated (Eq. 3) for each species based on drag force measurements at eight stream velocities between 0.02 and 0.37 m s^{-1} [13]. These velocities are in the range of stream velocities used in this research. In the second step, the experimental drag coefficient $C_{D,exp}$ is parameterized. The modified drag coefficient, C_D', obtained by (Eq. 3) is a function of stream velocity. It can be described by: $C_D' = C_{D,\exp}\left(\frac{U}{U_o}\right)^b$, with: the experimental drag coefficient, $C_{D,exp}$ (−), the Vogel number, b (−), the velocity, U (m s^{-1}), and U_0 has a constant value of 1 (m s^{-1}).

This approach is similar to the approach of Aberle, Jarvela [45] and Jarvela [5] who quantified the drag force. $C_{D,\exp}$ is a species-specific drag coefficient with a constant value, Table 1. Note that the flexible behaviour of the macrophytes is explicitly taken into account by the variable vegetation height depending on upstream depth-averaged velocity. The experimental drag coefficient is based on velocity measurements and it therefor only valid in this velocity range, 0.02–0.37 m s^{-1}. The use of the Vogel exponent and its interpretation is further discussed in Marjoribanks et al. [58].

2.3 Model description and calculation scheme

Telemac 2D is used to simulate water depths and depth-averaged stream velocities in both longitudinal and lateral direction [46]. This hydrodynamic model solves the depth-averaged Navier–Stokes equations for continuity and momentum simultaneously. The overall viscosity coefficient (molecular and turbulent viscosity) is constant for the entire model domain and equals 10^{-4} m^2 s^{-1}. A similar value is recommended to simulate accurately the sharp gradients of the depth-averaged velocity at the vegetation edges. This method already provides good results—as will be presented in the results section—showing that our simplified model approach is able to capture the most important processes determining the flow field in and around macrophyte patches at the studied scale. Specific models to simulate turbulence within aquatic vegetation are available. For example, King et al. [59] developed a k-ε model to simulate the turbulent kinetic energy generation and dissipation in interaction with vegetation, incorporating turbulence effects at stem scale and at scales of the vertical shear. In this study we chose to not take into account the turbulence effects due to the presence of vegetation, in order to keep the model as simple as possible.

A triangular regular grid with a node interval of 0.1 m is used. The boundary conditions are a constant discharge at the upstream boundary and a constant water depth downstream. Despite the grid size being small, a substantial amount of vegetation area is present in each grid cell and is between 852 and 4290 cm^2. The Chézy coefficient for the bed roughness (C_b) is obtained from standardised tables [51] and validated for an empty flume: this was 48 $m^{1/2}$ s^{-1} for the laboratory flume experiment and 20 $m^{1/2}$ s^{-1} for the in situ field flume.

Equation 2 quantifies the hydraulic roughness in function of the water depth in every grid cell; this matrix is then used as input in the hydrodynamic model. The calculation scheme is as follows: firstly, the boundary conditions of the system are defined and the depth-averaged velocity in an empty flume is calculated at the location upstream of the vegetation patch; then the deflected plant height is calculated, given this upstream depth-averaged velocity. Next, the representative Chézy value is calculated according to (Eq. 2) in every vegetated grid cell, which is used as input in the hydrodynamic model. In case of multiple vegetation patches an iterative approach is suggested. Initially the depth-averaged velocity is used to calculate the C_r of all patches. This initial C_r value should be used then to rerun the hydrodynamic model and to recalculate the depth-averaged velocity. In the next iteration, the depth-averaged velocity immediately upstream of each patch should be used to recalculate C_r. This is repeated until the flow field and C_r are in balance.

2.4 Case studies

The first case study consists of the modelling of experiments done by Bal et al. [4] (Fig. 2a). They investigated the influence of different macrophyte distribution patterns on the overall hydraulic resistance in a laboratory flume (25 m long, 3 m wide, 0.3 m water

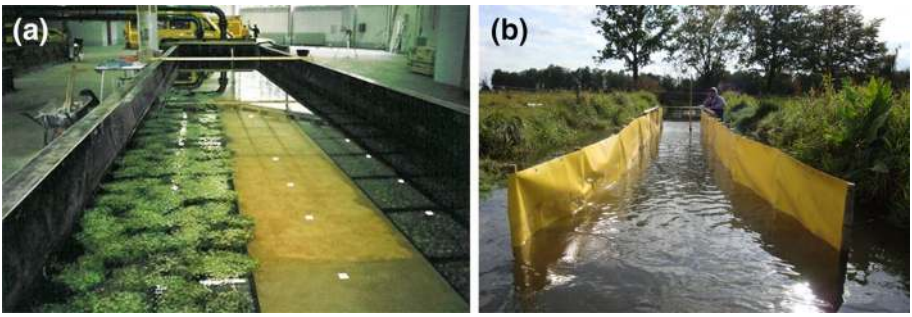

Fig. 2 **a** Illustration of the laboratory flume of Bal et al. [4], and **b** the in situ field flume of Schoelynck et al. [38]

depth). The velocity was measured over a time interval of 30 s (Valeport 801 electromagnetic flow meter) at 65 locations, of which 26 inside the vegetation, 13 at the edge and 26 next to the vegetation. At every location, 5 measurements were done with a depth interval of 0.05 m. No vegetation was present in the first 9 m of the flume, to create a uniform velocity profile across the upstream boundary. The configuration of one vegetation patch of 9 m by 1 m along the side wall of the flume was selected for this study. Three macrophyte species (*C. platycarpa, P. pectinatus* and *P. natans)* at three discharges (0.063, 0.095 and 0.127 $m^3\ s^{-1}$) are modelled, hence the first case study includes nine scenarios. The observed stream velocities are depth-averaged at each measurement location and are spatially, linearly interpolated in Akima's algorithm in R ver. 3.0 [60].

The second case study is an in situ field flume experiment, with *C. platycarpa*, performed by Schoelynck et al. [38] (Fig. 2b). The authors investigated the bending of patches as a result of the upstream depth-averaged velocity. A flume was placed in a lowland river in north east Belgium, creating a test section of 4.8 m long and 1 m wide. A vegetation free zone of 5 m upstream of the test section was installed to obtain a uniform velocity across the upstream boundary. The incoming discharge was 0.057 $m^3\ s^{-1}$; upstream and downstream water depth was 0.43 m and 0.68 m, respectively. At 26 locations in the flume the velocity was measured with an electromagnetic flow meter (Valeport 801) during 30 s. The depth-averaged stream velocities were calculated from measurements with a depth-interval of 0.1 m and afterwards spatially, linearly interpolated using Akima's algorithm.

3 Results

3.1 How to estimate the hydraulic resistance of in-stream macrophytes patches including temporary reconfiguration and based on measurable plant parameters? And is the resulting flow field in agreement with the observed flow field?

The observed depth-averaged stream velocities of the laboratory flume are plotted versus the modelled stream velocities to illustrate the model performance (Fig. 3). This is done for the 65 locations where the velocity was measured, respectively, for each combination of three macrophyte species and three discharges (Fig. 3). Error bars of the observed depth-averaged velocity represent the mean standard error based on the individual standard

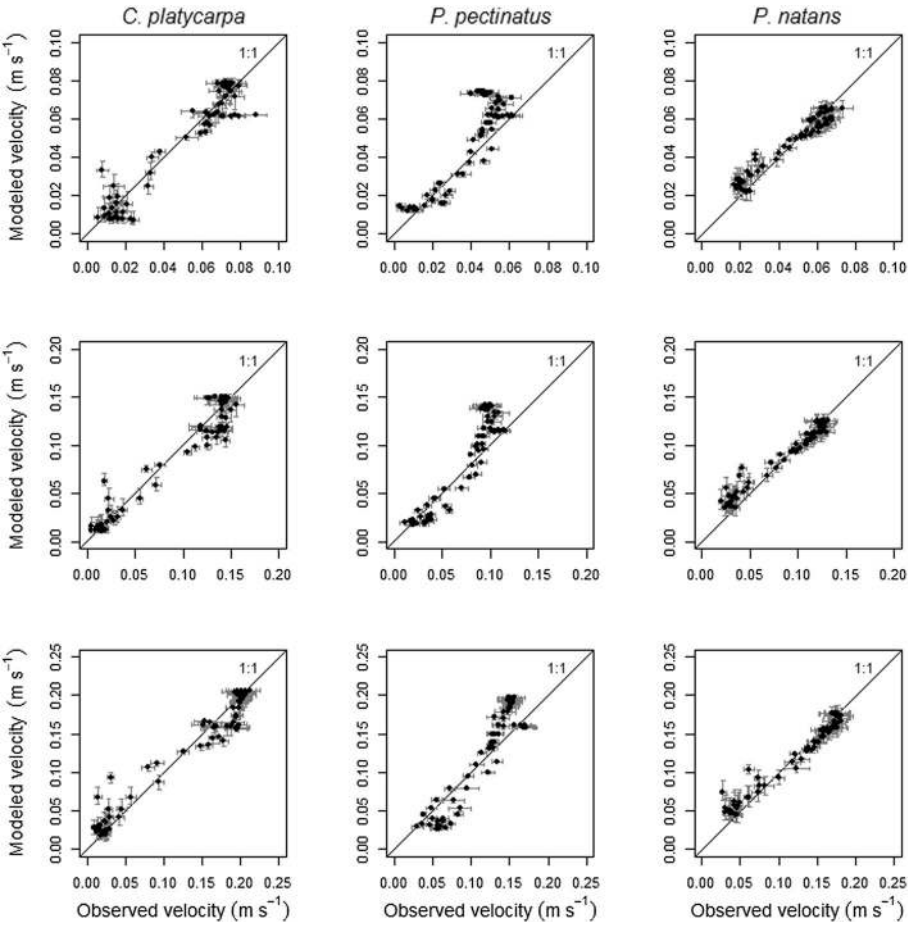

Fig. 3 Observed depth-averaged velocity versus modelled depth-averaged velocity for *C. platycarpa* (*first column*), *P. pectinatus* (*second column*) and *P. natans* (*third column*). The discharge is 0.063, 0.095 and 0.127 $m^3\ s^{-1}$ for the first, second and third row, respectively. The *black line* represents the 1:1-line. *Error bars* of the observed depth-averaged velocity represent the mean standard error based on the individual standard deviations of the 5 measured velocities at each location. The C_r is calculated by once subtracting, and once summing, the input parameters A_w and C_D' with their respective standard deviation. Depth-averaged velocities are modelled accordingly and are shown as error bars of the modelled depth-averaged velocity per location

deviations of the 5 measured stream velocities at each location. The C_r is calculated by once subtracting, and once summing, the input parameters A_w and C_D' with their respective standard deviation. Depth-averaged velocities are modelled accordingly and are shown as error bars of the modelled depth-averaged velocity per location (Fig. 3). A good fit gives points around the 1:1-line, most points lie close to the 1:1-line in each scenario. In all simulations of *C. platycarpa*, one point—in the left lower corner of the plot—is highly overestimated by the model. This point is situated at the upstream edge of the vegetation patch. In the panels of *P. pectinatus* a set of 6 points is overestimated by the model; these points are located in the channel next to the vegetation patch. In the simulation of *P. natans*

the model performance of small stream velocities is poorer; these points are located at the upstream edge of the vegetation patch.

For the nine scenarios, the coefficients of determination between modelled and observed depth-averaged velocities are all higher than 0.89 (Table 2). The mean absolute error and the root mean squared error do not exceed 0.023 m s^{-1} in all scenario's and are similar across species and discharges. The coefficient of variation—the relative error between observed and modelled data—is between 0.10 and 0.26 for all model scenarios. The Nash-Sutcliff coefficients are higher than 0.91 for the scenarios with *C. platycarpa* and *P. natans*, and lower for scenarios with *P. pectinatus*, but still higher than 0.39. The weaker performance of the scenarios with *P. pectinatus* can be due to an underestimation of the representative Chézy value, which results in lower stream velocities in the patch and higher stream velocities adjacent to the patch. Overall we can conclude that the model performs well in reproducing the observed depth-averaged velocity patterns and magnitudes for these conditions without any calibration of the parameters.

The scenario of *C. platycarpa* at a discharge of 0.127 m^3 s^{-1} is now discussed in detail, the other scenarios have similar results. The spatial distribution of the depth-averaged velocity is plotted in Fig. 4a based on the observed data (measurements available for only part of the flume) and based on the model simulations in Fig. 4b (modelled for the whole flume). The depth-averaged velocity at the location of the patch drops to 0.01 m s^{-1} in the observed and modelled data, though the actual velocity is lower inside the vegetation layer and is higher above the vegetation in the free flowing zone. The magnitude of the depth-averaged velocity adjacent to the patch increases to 0.20 m s^{-1} for the modelled data, which is comparable to the observed value of 0.21 m s^{-1}.

The modelled depth-averaged velocities show a slowdown along the vegetated longitudinal-section (Fig. 4c, black). The values of the modelled data are in line with those of the observed data. The increase in depth-averaged velocity in the open channel adjacent to the vegetation patch is slightly underestimated at the first part of the vegetation patch: the modelled depth-averaged velocity is 0.015 m s^{-1} lower than observed (Fig. 4c, grey). A

Table 2 Comparison between observed data and modelled data for a laboratory flume experiment: coefficient of determination (R^2), mean absolute error (MAE), root mean squared errors (RMSE), coefficient of variation (CV = RMSE/u_{avg}) and Nash-Sutcliff model efficiency coefficient $\left(NS = 1 - \frac{\sum_{i=1}^{n}\left(u_{m,i} - u_{o,i}\right)^2}{\sum_{i=1}^{n}\left(u_{o,i} - u_{o,avg}\right)^2}\right)$ with $u_{o,avg}$ = mean depth-averaged observed velocity and n = number of paired observed-modelled stream velocities

Species	Discharge (m^3 s^{-1})	R^2 (–)	MAE (m s^{-1})	RMSE (m s^{-1})	CV (–)	NS (–)
C. platycarpa	0.063	0.96	0.006	0.008	0.16	0.91
	0.095	0.97	0.011	0.015	0.17	0.93
	0.127	0.97	0.014	0.019	0.16	0.94
P. pectinatus	0.063	0.89	0.010	0.013	0.26	0.39
	0.095	0.93	0.018	0.023	0.26	0.48
	0.127	0.94	0.023	0.027	0.23	0.63
P. natans	0.063	0.97	0.004	0.005	0.10	0.92
	0.095	0.98	0.008	0.011	0.14	0.93
	0.127	0.98	0.010	0.013	0.11	0.94

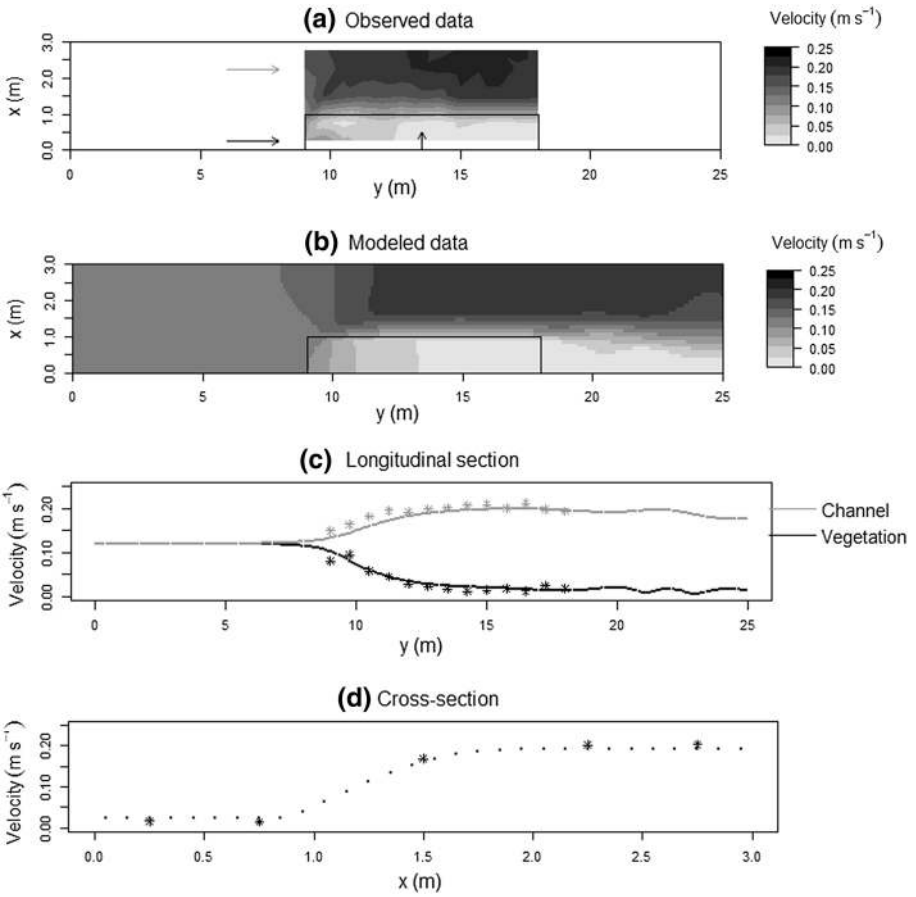

Fig. 4 Spatial distribution of the depth-averaged velocity of the observed data (**a**) and modelled data (**b**) for *C. platycarpa* at a discharge of 0.127 $m^3 s^{-1}$. The vegetation patch is demarked with a *black line* in (**a**) and (**b**). The water flows from *left* to *right*. The *arrows* in (**a**) indicate the location of the cross-section in the middle of the patch, which are displayed in (**d**), and the longitudinal transects displayed in (**c**); one through the vegetation (*black*) and one adjacent to the vegetation (*grey*). The modelled data are represented by *circles* and the observed data by stars in (**c**) and (**d**)

similar trend is noticed along the cross-section: the depth-averaged velocity is slowed down in the part through the vegetation, while the depth-averaged velocity increased around the vegetation (Fig. 4d). The modelled depth-averaged velocities are also in line with the observations.

3.2 What is the effect of inclusion or exclusion of macrophyte reconfiguration on the modelled flow field?

The flow field is now simulated with and without reconfiguration for an in situ field flume experiment [38]. The total biomass and rooted area of the vegetation patch is the same in both scenarios, so an equal amount of vegetation is present in both scenarios. The plant height is calculated with the bending angles of Table 1. The free flowing calculated zone

above the canopy is 0.08 m in the scenario after reconfiguration and similar to the field observation of 0.1 m, while the vegetation is considered to remain in upright position in the scenario without reconfiguration (Fig. 5). Note that the patch length is longer with reconfiguration due the bending.

In contrast to the flat bottom of the laboratory flume, the river bottom of the in situ field flume had a significant bottom slope, with a higher water depth at the end of the flume. As a result a decreasing depth-averaged velocity towards the end of the flume is observed (Fig. 5a) and accurately simulated by the model in the scenario with reconfiguration (Fig. 5b). The depth-averaged velocity at the downstream end of the patch drops to 0.06 m s^{-1} in the observed data and to 0.07 m s^{-1} in the modelled data. It can be seen from the data in Fig. 4b that the depth-averaged velocity in the open channel increases to 0.11 m s^{-1}. In the observed data, the depth-averaged velocity is 0.16 m s^{-1} at one location. Without implementing reconfiguration, the flow field shows more extreme values (Fig. 5c): a higher depth-averaged velocity adjacent to the patch, 0.19 m s^{-1}, and a lower depth-averaged velocity behind the patch, 0.05 m s^{-1}. Furthermore, the decreased depth-averaged velocities in the patch already start at the upstream edge of the patch; while, when reconfiguration is implemented, the depth-averaged velocity gradually decreases through the patch.

The modelled data with reconfiguration are in better agreement with the observed data compared to the scenario without reconfiguration (Table 3). The correlation coefficient and

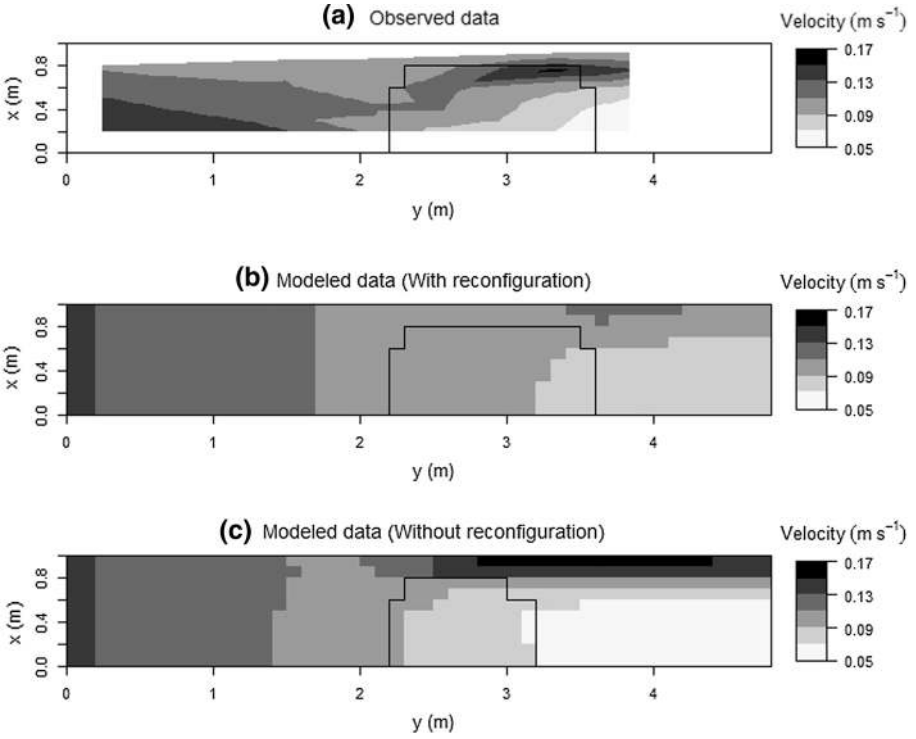

Fig. 5 Spatial distribution of the depth-averaged velocity of the observed data (**a**) and modelled data with (**b**) and without (**c**) reconfiguration for the in situ field flume. The vegetation patch is demarked with a *black line* in (**a**), (**b**) and (**c**). The water flows from *left* to *right*

Table 3 Comparison between observed data and modelled data with and without reconfiguration of an in situ flume with a patch of *C. platycarpa*: coefficient of determination (R^2), mean absolute error (MAE), root mean squared errors (RMSE), coefficient of variation (CV) and Nash-Sutcliff model efficiency coefficient (NS)

Species	Reconfiguration	R^2 (–)	MAE (m s^{-1})	RMSE (m s^{-1})	CV (–)	NS (–)
C. platycarpa	Yes	0.74	0.014	0.017	0.17	0.52
C. platycarpa	No	0.63	0.016	0.023	0.23	0.16

Nash-Sutcliff coefficient are both higher in the case that reconfiguration of the canopy is implemented in the model. In addition, the mean absolute error, root mean squared error and the coefficient of variation, are lower with the inclusion of macrophyte reconfiguration.

The distribution of the stream velocities per water volume is calculated to have more detailed information on how the flow field is changed by the vegetation. The depth-averaged velocity distribution of the model simulation, with the inclusion of reconfiguration, peaks at the interval of 0.10 to 0.12 m s^{-1} (Fig. 6), with 46.2 % of the water volume having this depth-averaged velocity. While two peaks are observed in the simulation without reconfiguration: 31.3 % of the water volume is in the interval 0.10–0.12 m s^{-1} and 25 % is in the interval 0.04–0.06 m s^{-1}. Next, the range of stream velocities is higher without reconfiguration 0.04 and 0.16 m s^{-1}, compared to the simulation with reconfiguration 0.06 and 0.14 m s^{-1}. More extreme values are observed without reconfiguration, the water volumes with a depth-averaged velocity lower than 0.06 m s^{-1} and higher than 0.14 m s^{-1} are 8.5 and 7.2 %, respectively.

4 Discussion

The majority of mathematical studies and experiments to quantify hydraulic resistance created by aquatic vegetation does not consider vegetation with natural characteristics but simplifies it to e.g. rigid sticks [e.g. 1, 6, 11, 31], horsehair matrasses [e.g. 61] or flexible plastic strips [e.g. 12, 39, 62, 63]. However, natural macrophytes are flexible and have more complex morphology compared to the former objects. In this study, we quantify the hydraulic roughness of natural submerged flexible macrophytes with a complex morphology using (Eq. 2) [1]. Vegetation was originally represented by rigid sticks, thus two

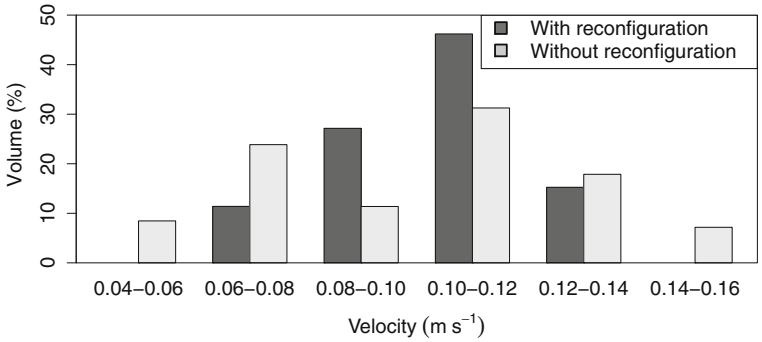

Fig. 6 Water volume (%) with according depth-averaged velocity, for the model simulation with macrophyte reconfiguration and without, of an in situ flume with a patch of *C. platycarpa*

adjustments are needed: (i) to account for the flexibility of the vegetation, the vegetation canopy height is varied as a function of the upstream depth-averaged velocity, and (ii) the morphology is represented by the total wetted surface area (A_w) of the plants. These parameters are estimated for three different macrophytes species (Table 1) and the proposed method is successfully validated against experimental data (Figs. 3, 4, 5). Next, we demonstrate that the incorporation of macrophyte reconfiguration in hydrodynamic river modelling results in a more realistic simulation of the observed depth-averaged velocity distribution (Fig. 6).

The approach presented in this study has three main advantages. Firstly, the plant parameters have a physical meaning and can be measured on natural macrophytes; this removes the need of further calibration of the hydraulic roughness. Secondly, the calculated hydraulic roughness created by vegetation is represented by an adapted bottom friction coefficient and hence can be used as input in existing hydrodynamic models. Lastly, a 2D depth-averaged model is used to directly account for the spatial variation in vegetated reaches and makes it possible to study spatial heterogeneous patterns.

However, the method presented in this paper also has limitations. It should be noted that macrophyte reconfiguration is described by the temporary bending of the vegetation which results in varying vegetation height in function of upstream depth-averaged velocity. This approach is therefore only valid for flexible vegetation, for which reconfiguration of the canopy results mainly in variation in vegetation height. Currently the vegetation resistance file is a fixed input in the hydrodynamic model based on the upstream depth-averaged velocity, thus new resistance files need to be calculated whenever the upstream depth-averaged velocity changes. Furthermore, Bal et al. [4] showed that stream velocity patterns also depend on the spatial configuration of vegetation patches and on water depth. The case studies presented in this study only contained one vegetation patch at one water depth. Future model application should study the accuracy of the proposed formulations in more complex multi-patch simulations. Finally, several limitations are inherent to 2D models. As a consequence of the 2D model approach, it is not possible to derive the stream velocities in and above the vegetation separately. Also, detailed 3D processes are expected to occur around finite submerged vegetation patches [15, 64]; vertical circulation patterns and expansion of mixing layers are, however, not captured by the presented 2D model. Skimming flow results in flow separation within and above the canopy, with reduce flow within the canopy and a boundary layer developing above the canopy [65]. This process is indirectly taken into account by the two layer formulation of (Eq. 1).

Notwithstanding two adjustments, the proposed method is able to accurately simulate the depth-averaged stream velocities for nine scenarios of a laboratory flume experiment (Figs. 3, 4). The hydraulic roughness of the vegetation results in a flow deceleration through—and downstream of—the vegetation, and an acceleration adjacent to the vegetation [2, 38]. The magnitude of velocity changes depends on the morphology and flexibility of the macrophyte species [13, 66]. The highest resistance is created by the most dense species *C. platycarpa,* for which the spatial variation depth-averaged velocity ranged between 0.01 and 0.16 m s^{-1} at discharge 0.095 m^3 s^{-1}. A similar impact on the stream velocity is found for *Callitriche cophocarpa* [16]. *P. pectinatus* is a less densely growing macrophyte and *P. natans* is the least dense species, hence the depth-averaged velocity range at the same discharge between 0.02 and 0.12 m s^{-1} and 0.03 and 0.14 m s^{-1}, respectively. These differences between the three target species are well simulated with the model (Fig. 3).

Here, we discuss that including macrophyte reconfiguration in the input of numerical models can have significant and extensive effects on the model results of hydrodynamic

variables and associated ecological and geomorphological parameters. This is illustrated by the simulation of the in situ field flume. The values presented are indicative and cannot be directly extrapolated to bigger spatial scales like reaches or entire rivers. Presumably the importance of the reconfiguration of the vegetation will become more pronounced as the real river morphology is taken into account and the number of patches increases.

In this study, reconfiguration is described by a variable vegetation height. Including reconfiguration, results in a free flowing zone above the canopy of 0.08 m, while it disappears in cases without reconfiguration. The magnitude of this zone affects the hydraulic roughness and hence the depth-averaged velocity distribution (Fig. 6). A smaller variation of the depth-averaged velocities, with less deceleration of the velocity through the patch and less acceleration around the patch (Table 4) is observed when reconfiguration is included. A second example is a decreased water level slope with reconfiguration (Table 4). The water level slope is the difference between the average water level, across the upstream and downstream boundary, divided by the flume length. Thirdly, we calculated the reach averaged hydraulic resistance expressed by a Manning coefficient. This is lower when the model accounts for macrophyte reconfiguration (Table 4). Therefore, the overall resistance created by the vegetation increases without reconfiguration. This finding is in agreement with previous studies, which also found that the impact of the vegetation becomes less pronounced with increasing free flowing zones above the canopy [61, 67, 68]. However, small values of the Manning coefficient are recorded; this is probably due to significant bottom slope which results in lower depth-averaged stream velocities towards the downstream end of the flume.

The maximal depth-averaged velocity adjacent to the patch is the first example of an ecological parameter. It is 0.13 m s^{-1} with reconfiguration, compared to 0.19 m s^{-1} without reconfiguration. This higher stream velocity can have severe impacts on plant performance during several life stages, such as: (i) settlement of seeds; (ii) survival rate and growth of propagules; and (iii) breakage of entire plants. Firstly, Koch et al. [73] tested the effect of flow velocity on horizontal dispersion distance of seeds of three macrophyte species in a flume experiment. It was found that the dispersion distance significantly

Table 4 Values of the investigated hydraulic, ecological and geomorphological parameters calculated based on the model scenario, with and without the inclusion of macrophyte reconfiguration of an in situ flume, with a patch of *C. platycarpa*. u_{95} = 95 percentile of velocities between 2.4 m and 4.8 m of the study section; D_{50} = 167 μm; D_{84} = 280 μm

Parameter	Reference	With reconfiguration	Without reconfiguration	Units
Hydraulics				
Depth averaged velocity (range)	Model ouptut	0.07–0.13	0.05–0.19	m s^{-1}
Water level slope	Model output	6.7×10^{-6}	162×10^{-6}	m m^{-1}
Manning coefficient	[69]	0.011	0.048	s $m^{-1/3}$
Ecology				
Maximal depth-averaged velocity	Model output	0.13	0.19	m s^{-1}
Macro-invertebrate drift at u_{95}	[70]	III (<0.2 m s^{-1})	III (<0.2 m s^{-1})	–
Geomorphology				
Shear stress at u_{95}	[71]	0.37	0.73	N m^{-2}
Bedload transport rate at u_{95}	[71]	0.24	0.25	g m^{-1} s^{-1}
Shield parameter at u_{95}	[72]	4.5	9.5	–

increased for current velocities above 0.2 m s^{-1}. Longer dispersion distance reduces the probability of seeds to remain in suitable habitats that were already colonised by the parent plants. Secondly, the survival rate of *C. platycarpa* was measured by transplanting propagules within and adjacent to existing patches of the same species [8]. It was found that both survival and growth were significantly lower, adjacent to the patch. These differences were attributed to difference in flow velocity. Thirdly, macrophytes experience drag force, which can lead to stem breakage [74]. The magnitude of the drag force depends on the flow velocity. An overestimation of prevailing stream velocities, adjacent to the patch when reconfiguration is not taken into account, could therefore lead to incorrect predictions of plant performance—as discussed above. In a second ecological example, Extence et al. [70] categorises the occurrence of benthic macro-invertebrates based on the prevailing stream velocities in rivers. Category I represents the highest stream velocities that are a habitat to rheophilic species (i.e. species preferring zones with high flow velocities), whereas categories III to VI represent low velocities suitable to limnophilic species (i.e. species preferring zones with low flow velocities). From our results it was found that, with the inclusion of macrophyte reconfiguration, the stream velocities do not exceed the threshold stream velocity of 0.2 m s^{-1} (Table 4); thus all taxa of category III are able to tolerate these conditions' taxa. The stream velocities of both scenarios in cases belong to the same category. However, simulated depth-averaged velocity, without implementing reconfiguration, can exceed the threshold value of 0.2 m s^{-1} more rapidly in cases with higher incoming stream velocities or other macrophyte species.

Macrophytes also influence the geomorphology of the river bed [9, 75], higher velocities adjacent to patch might lead to scouring or grain sorting. Firstly, the maximum values for the bed shear stress are 0.37 and 0.73 N m^{-2} (Table 4), respectively, with and without the inclusion of macrophyte reconfiguration. Schoelynck et al. [38] showed that a minimal bed shear stress of 0.15–0.16 N m^{-2} is needed to initiate sediment motion in the in situ flume, with prevailing median grain size of 0.167 mm [38]. Secondly, the sediment bed load transport rate based on the bed shear stress is, respectively, 0.25 and 0.24 g m^{-1} s^{-1}, without and with the inclusion of macrophyte reconfiguration (Table 4). Note that for the calculation of the shear stress and sediment bed load transport the depth-averaged velocity is used instead of the near bed velocity. Near bed velocities are expected to be lower and resulting in a lower shear stress and lower bed load transport. However, we want to illustrate the effect of difference in depth-averaged stream velocities between inclusion and exclusion of reconfiguration; therefore, the difference between the two scenarios is more important than the absolute values. Finally, the Shield parameter is the ratio of the actual forces acting on sediment and the forces needed to initiate sediment motion [72]. The values for the scenarios with and without reconfiguration are 4.5 and 9.5, respectively. These values are both higher than 1; this implies the movement of sediment adjacent to the macrophyte patch, but with a different magnitude.

5 Conclusion

The aim of this study is to derive a practical approach to quantify vegetation resistance which can be applied in 2D depth-averaged hydrodynamic models on reach scale. The hydraulic resistance created by flexible in-stream macrophytes with a complex morphology is represented by an adapted bottom friction coefficient. Measurable plant parameters are derived and quantified to account for the variable vegetation height and complex

morphology of three submerged macrophyte species. This approach removes the need for calibration of the vegetation resistance and can be applied in reaches with spatial heterogeneous vegetation patterns. This study has three major findings: (i) the model is able to accurately predict the depth-averaged velocities in and around a vegetation patch, by implementing the vegetation resistance into the hydrodynamic model Telemac 2D without calibration of any parameter. (ii) The flexible vegetation approach is superior to a fixed vegetation height. Inclusion of macrophyte reconfiguration in the model decreases the simulated hydraulic resistance which results in less variation in the simulated depth-averaged velocity distribution as compared to the model scenario without macrophyte reconfiguration. (iii) Inclusion or exclusion of macrophyte reconfiguration can have significant and extensive effects on the model results of hydrodynamic variables and associated ecological and geomorphological parameters. This implies that more attention should be paid to the variable vegetation height in hydrodynamic models when dealing with flexible, submerged macrophytes.

Acknowledgments Data used in this paper can be accessed via the authors (veerle.verschoren@uantwerpen.be). V.V. thanks the Institute for the Promotion of Innovation through Science and Technology in Flanders (IWT-Vlaanderen) for personal research funding. D.M. would like to thank BOF (Bijzonder Onderzoeksfonds, UGhent) for funding personal research. J.S. is a postdoctoral fellow of FWO (project no. 12H8616N). K.D.B. would like to acknowledge the financial support of the South African National Research Foundation (NRF). This research was partly executed with the financial support of the FWO for the Scientific Research Network (WOG) "the functioning of river ecosystems through plant-flow-soil interactions".

References

1. Baptist MJ, Babovic V, Uthurburu JR, Keijzer M, Uittenbogaard RE, Mynett A, Verwey A (2007) On inducing equations for vegetation resistance. J Hydraul Res 45(4):435–450
2. Vandenbruwaene W, Temmerman S, Bouma TJ, Klaassen PC, de Vries MB, Callaghan DP, van Steeg P, Dekker F, van Duren LA, Martini E, Balke T, Biermans G, Schoelynck J, Meire P (2011) Flow interaction with dynamic vegetation patches: implications for biogeomorphic evolution of a tidal landscape. J Geophys Res-Earth. doi:10.1029/2010jf001788
3. Zong LJ, Nepf H (2010) Flow and deposition in and around a finite patch of vegetation. Geomorphology 116(3–4):363–372. doi:10.1016/j.geomorph.2009.11.020
4. Bal KD, Struyf E, Vereecken H, Viaene P, De Doncker L, de Deckere E, Mostaert F, Meire P (2011) How do macrophyte distribution patterns affect hydraulic resistances? Ecol Eng 37(3):529–533. doi:10.1016/j.ecoleng.2010.12.018
5. Jarvela J (2005) Effect of submerged flexible vegetation on flow structure and resistance. J Hydrol 307(1–4):233–241. doi:10.1016/j.jhydrol.2004.10.013
6. Nepf HM (2012) Hydrodynamics of vegetated channels. J Hydraul Res 50(3):262–279
7. Franklin P, Dunbar M, Whitehead P (2008) Flow controls on lowland river macrophytes: a review. Sci Total Environ 400(1–3):369–378. doi:10.1016/j.scitotenv.2008.06.018
8. Schoelynck J, De Groote T, Bal K, Vandenbruwaene W, Meire P, Temmerman S (2012) Self-organised patchiness and scale-dependent bio-geomorphic feedbacks in aquatic river vegetation. Ecography 35(8):760–768. doi:10.1111/j.1600-0587.2011.07177.x
9. Gurnell AM (2014) Plants as river system engineers. Earth Surf Process Landf 39(1):4–25
10. Huthoff F, Augustijn DCM, Hulscher SJMH (2007) Analytical solution of the depth-averaged flow velocity in case of submerged rigid cylindrical vegetation. Water Resour Res. doi:10.1029/2006wr005625
11. Zhang ML, Li CW, Shen YM (2013) Depth-averaged modeling of free surface flows in open channels with emerged and submerged vegetation. Appl Math Model 37(1–2):540–553. doi:10.1016/j.apm.2012.02.049
12. Ortiz AC, Ashton A, Nepf H (2013) Mean and turbulent velocity fields near rigid and flexible plants and the implications for deposition. J Geophys Res-Earth 118(4):2585–2599. doi:10.1002/2013jf002858

13. Bal KD, Bouma TJ, Buis K, Struyf E, Jonas S, Backx H, Meire P (2011) Trade-off between drag reduction and light interception of macrophytes: comparing five aquatic plants with contrasting morphology. Funct Ecol 25(6):1197–1205. doi:10.1111/j.1365-2435.2011.01909.x
14. Nepf HM, Ghisalberti M (2008) Flow and transport in channels with submerged vegetation. Acta Geophys 56(3):753–777. doi:10.2478/s11600-008-0017-y
15. Nikora N, Nikora V (2010) Flow penetration into the canopy of submerged vegetation: definitions and quantitative estimates. In: Dittrich AK, Koll K, Aberle J, Geisenhainer P (eds) River flow 2010. Federal Waterways Engineering and Research Insitute, Karlsruhe, pp 437–444
16. Sand-Jensen K, Pedersen ML (2008) Streamlining of plant patches in streams. Freshw Biol 53(4):714–726. doi:10.1111/j.1365-2427.2007.01928.x
17. De Doncker L, Troch P, Verhoeven R, Bal K, Meire P, Quintelier J (2009) Determination of the Manning roughness coefficient influenced by vegetation in the river Aa and Biebrza river. Environ Fluid Mech 9(5):549–567. doi:10.1007/s10652-009-9149-0
18. Dawson FH (1978) Aquatic plant management in semi-natural streams: role of marginal vegetation. J Environ Manag 6(3):213–221
19. Green JC (2005) Comparison of blockage factors in modelling the resistance of channels containing submerged macrophytes. River Res Appl 21(6):671–686. doi:10.1002/Rra.854
20. Van Ieperen HJ, Herfst MS (1986) Laboratory experiments on the flow resistance of aquatic weeds. In: 2nd international conference on hydraulic design in water resources engineering: land drainage, pp 281–291
21. Temple DM (1986) Velocity distribution coefficients for grass-lined channels. J Hydraul Eng 112(3):193–205
22. Larsen T, Frier JO, Vestergaard K (1990) Discharge stage relations in vegetated danish streams. In: international conference on river flood hydraulics, pp 187–195
23. Bakry MF, Gates TK, Khattab AF (1992) Field-measured hydraulic resistance characteristics in vegetation-infested canals. J Irrig Drain Eng 118(2):256–274. doi:10.1061/(Asce)0733-9437(1992)118:2(256)
24. Stone BM, Shen HT (2002) Hydraulic resistance of flow in channels with cylindrical roughness. J Hydraul Eng 128(5):500–506. doi:10.1061/(Asce)0733-9429(2002)128:5(500)
25. Wilson CAME, Stoesser T, Bates PD, Pinzen AB (2003) Open channel flow through different forms of submerged flexible vegetation. J Hydraul Eng 129(11):847–853. doi:10.1061/(Asce)0733-9429(2003)129:11(847)
26. Vargas-Luna A, Corsato A, Uijttewaal WSJ (2015) Effects of vegetation on flow and sediment transport: comparative analyses and validation of prediction models. Earth Surf Proc Land 40:157–176. doi:10.1002/esp.3633
27. de Langre E, Gutierrez A, Cossé J (2012) On scaling of drag reduction by reconfiguration in plants. Comptes Rendus Mech 340:35–40. doi:10.1016/j.crme.2011.11.005
28. Folkard AM (2011) Vegetated flows in their environmental context: a review. Proceedings of the ICE - Engineering and Computational Mechanics 164(1):3–24. doi:10.1680/eacm.8.00006
29. Nepf HM (1999) Drag, turbulence, and diffusion in flow through emergent vegetation. Water Resour Res 35(2):479–489
30. Jarvela J (2002) Flow resistance of flexible and stiff vegetation: a flume study with natural plants. J Hydrol 269(1–2):44–54
31. Chen ZB, Jiang CB, Nepf H (2013) Flow adjustment at the leading edge of a submerged aquatic canopy. Water Resour Res 49(9):5537–5551. doi:10.1002/Wrcr.20403
32. Wu F (2007) Characteristics of flow resistance in floodplain with non-submerged rigid vegetation. Asian Pac Coasts 2007:387–390
33. do Amaral LGH, Righes AA, Souza PD, Dalla Costa R (2005) Automatic regulator for channel flow control on flooded rice. Agric Water Manag 75(3):184–193. doi:10.1016/j.agwat.2004.12.012
34. Tal M, Paola C (2007) Dynamic single-thread channels maintained by the interaction of flow and vegetation. Geology 35(4):347–350. doi:10.1130/G23260a.1
35. Horppila J, Nurminen L (2003) Effects of submerged macrophytes on sediment resuspension and internal phosphorus loading in Lake Hiidenvesi (southern Finland). Water Res 37(18):4468–4474. doi:10.1016/S0043-1354(03)00405-6
36. Nikora V (2010) Hydrodynamics of aquatic ecosystems: an interface between ecology, biomechanics and environmental fluid mechanics. River Res Appl 26(4):367–384. doi:10.1002/Rra.1291
37. Puijalon S, Bornette G, Sagnes P (2005) Adaptations to increasing hydraulic stress: morphology, hydrodynamics and fitness of two higher aquatic plant species. J Exp Bot 56(412):777–786. doi:10.1093/Jxb/Eri063

38. Schoelynck J, Meire D, Bal K, Buis K, Troch P, Bouma T, Meire P, Temmerman S (2013) Submerged macrophytes avoiding a negative feedback in reaction to hydrodynamic stress. Limnologica 43(5):371–380. doi:10.1016/j.limno.2013.05.003
39. Dijkstra JT (2009) How to account for flexible aquatic vegetation in large-scale morphodynamic models. Coast Eng 1–5:2820–2831
40. Dijkstra JT, Uittenbogaard RE (2010) Modeling the interaction between flow and highly flexible aquatic vegetation. Water Resour Res. doi:10.1029/2010wr009246
41. Luhar M, Nepf HM (2011) Flow-induced reconfiguration of buoyant and flexible aquatic vegetation. Limnol Oceanogr 56(6):2003–2017. doi:10.4319/lo.2011.56.6.2003
42. Siniscalchi F, Nikora VI (2012) Flow-plant interactions in open-channel flows: a comparative analysis of five freshwater plant species. Water Resour Res. doi:10.1029/2011wr011557
43. Folkard AM (2005) Hydrodynamics of model Posidonia oceanica patches in shallow water. Limnol Oceanogr 50(5):1592–1600
44. Siniscalchi F, Nikora VI, Aberle J (2012) Plant patch hydrodynamics in streams: mean flow, turbulence, and drag forces. Water Resour Res. doi:10.1029/2011wr011050
45. Aberle J, Jarvela J (2013) Flow resistance of emergent rigid and flexible floodplain vegetation. J Hydraul Res 51(1):33–45. doi:10.1080/00221686.2012.754795
46. Hervouet J-M (2007) Hydrodynamics of free surface flows: modelling with the finite element method. Wiley, West Sussex
47. Vargas-Luna A, Corsato A, Uijttewaal WSJ (2015) Effects of vegetation on flow and sediment transport: comparative analyses and validation of prediction models. Earth Surf Proc Land. doi:10.1002/esp.3633
48. Arboleda AM, Crosato A, Middelkoop H (2010) Reconstructing the early 19th-century Waal River by means of a 2D physics-based numerical model. Hydrol Process 24(25):3661–3675. doi:10.1002/Hyp.7804
49. Crosato A, Saleh MS (2011) Numerical study on the effects of floodplain vegetation on river planform style. Earth Surf Proc Land 36(6):711–720. doi:10.1002/Esp.2088
50. Nardin W, Edmonds DA (2014) Optimum vegetation height and density for inorganic sedimentation in deltaic marshes. Nat Geosci 7(10):722–726. doi:10.1038/Ngeo2233
51. Ancrement GJ, Schneider VR (1989) Guide for selecting Manning's roughness coefficients for natural channels and flood plains. United States Government Printing Office, Washington
52. Jalonen J, Jarvela J, Aberle J (2013) Leaf area index as vegetation density measure for hydraulic analyses. J Hydraul Eng 139(5):461–469. doi:10.1061/(Asce)Hy.1943-7900.0000700
53. Schoneboom T, Aberle J, Dittrich A (2010) Hydraulic resistance of vegetated flows: contribution of bed shear stress and vegetative drag to total hydraulic resistance. In: Dittrich AK, Koll K, Aberle J, Geisenhainer P (eds) River flow 2010. Federal Waterways Engineering and Research Insitute, Karlsruhe, pp 269–276
54. Nepf HM (2012) Flow and transport in regions with aquatic vegetation. Annu Rev Fluid Mech 44:123–142. doi:10.1146/annurev-fluid-120710-101048
55. Sand-Jensen K (2003) Drag and reconfiguration of freshwater macrophytes. Freshw Biol 48(2):271–283. doi:10.1046/j.1365-2427.2003.00998.x
56. Hoerner S (1965) Fluid-dynamic drag. Hoerner Fluid Dynamics, Brick Town
57. Whittaker P, Wilson C, Aberle J, Rauch HP, Xavier P (2013) A drag force model to incorporate the reconfiguration of full-scale riparian trees under hydrodynamic loading. J Hydraul Res 51(5):569–580. doi:10.1080/00221686.2013.822936
58. Marjoribanks TI, Hardy RJ, Lane SN (2014) The hydraulic description of vegetated river channels: the weakness of existing formulations and emerging alternatives. WIREs Water 1(6):549–560. doi:10.1002/wat2.1044
59. King AT, Tinoco RO, Cowen EA (2012) A k-epsilon turbulence model based on the scales of vertical shear and stem wakes valid for emergent and submerged vegetated flows. J Fluid Mech 701:1–39. doi:10.1017/Jfm.2012.113
60. Akima H (2013) Akima: interpolation of irregularly spaced data. R package ver. 3.0
61. Wu F, Shen HW, Chou YJ (1999) Variation of roughness coefficients for unsubmerged and submerged vegetation. J Hydraul Eng 125(9):934–942. doi:10.1061/(Asce)0733-9429(1999)125:9(934)
62. Kouwen N, Li RM (1980) Biomechanics of vegetative channel linings. J Hydrual Eng Div 106(6):1085–1106
63. Ciraolo G, Ferreri GB, La Loggia G (2006) Flow resistance of Posidonia oceanica in shallow water. J Hydraul Res 44(2):189–202
64. Sukhodolova TA, Sukhodolov AN (2012) Vegetated mixing layer around a finite-size patch of submerged plants: 1. Theory and field experiments. Water Resour Res. doi:10.1029/2011wr011804

65. Folkard AM (2011) Flow regimes in gaps within stands of flexible vegetation: laboratory flume simulations. Environ Fluid Mech 11(3):289–306. doi:10.1007/s10652-010-9197-5
66. Bal KD, Brion N, Woule-Ebongue V, Schoelynck J, Jooste A, Barron C, Dehairs F, Meire P, Bouma TJ (2013) Influence of hydraulics on the uptake of ammonium by two freshwater plants. Freshw Biol 58(12):2452–2463. doi:10.1111/Fwb.12222
67. Stephan U, Gutknecht D (2002) Hydraulic resistance of submerged flexible vegetation. J Hydrol 269(1–2):27–43. doi:10.1016/S0022-1694(02)00192-0
68. Wilson CAME (2007) Flow resistance models for flexible submerged vegetation. J Hydrol 342(3–4):213–222. doi:10.1016/j.jhydrol.2007.04.022
69. Chow VT (1959) Open-channel hydraulics. McGraw-Hill, New York. doi:10.1029/TR037i003p00327
70. Extence CA, Balbi DM, Chadd RP (1999) River flow indexing using British benthic macroinvertebrates: a framework for setting hydroecological objectives. Regul River 15(6):543–574
71. Gibbins C, Vericat D, Batalla RJ (2007) When is stream invertebrate drift catastrophic? The role of hydraulics and sediment transport in initiating drift during flood events. Freshw Biol 52(12):2369–2384. doi:10.1111/j.1365-2427.2007.01858.x
72. Umeda S (2011) Scour regime and scour depth around a pile in waves. J Coast Res 64:845–849
73. Koch EW, Ailstock MS, Booth DM, Shafer DJ, Magoun AD (2010) The role of currents and waves in the dispersal of submersed angiosperm seeds and seedlings. Restor Ecol 18(4):584–595. doi:10.1111/j.1526-100X.2010.00698.x
74. Puijalon S, Bouma TJ, Douady CJ, van Groenendael J, Anten NPR, Martel E, Bornette G (2011) Plant resistance to mechanical stress: evidence of an avoidance-tolerance trade-off. New Phytol 191(4):1141–1149. doi:10.1111/j.1469-8137.2011.03763.x
75. Montakhab A, Yusuf B, Ghazali AH, Mohamed TA (2012) Flow and sediment transport in vegetated waterways: a review. Rev Environ Sci Bio-Technol 11(3):275–287. doi:10.1007/s11157-012-9266-y